Published OnlineFirst August 21, 2015; DOI: 10.1158/0008-5472.CAN-15-1107

Therapeutics, Targets, and Chemical Biology

Cancer Research

Identification of P450 Oxidoreductase as a Major Determinant of Sensitivity to Hypoxia-Activated Prodrugs

Francis W. Hunter[1], Richard J. Young[2,3], Zvi Shalev[4], Ravi N. Vellanki[4], Jingli Wang[1], Yongchuan Gu[1,5], Naveen Joshi[1], Sreevalsan Sreebhavan[1], Ilan Weinreb[4], David P. Goldstein[6], Jason Moffat[7], Troy Ketela[8], Kevin R. Brown[8], Marianne Koritzinsky[4,7,9], Benjamin Solomon[2,3,10], Danny Rischin[3,10], William R. Wilson[1], and Bradly G. Wouters[4,7,11,12]

Abstract

Hypoxia is a prevalent feature of many tumors contributing to disease progression and treatment resistance, and therefore constitutes an attractive therapeutic target. Several hypoxia-activated prodrugs (HAP) have been developed, including the phase III candidate TH-302 (evofosfamide) and the preclinical agent SN30000, which is an optimized analogue of the well-studied HAP tirapazamine. Experience with this therapeutic class highlights an urgent need to identify biomarkers of HAP sensitivity, including enzymes responsible for prodrug activation during hypoxia. Using genome-scale shRNA screens and a high-representation library enriched for oxidoreductases, we identified the flavoprotein P450 (cytochrome) oxidoreductase (POR) as the predominant determinant of sensitivity to SN30000 in three different genetic backgrounds. No other genes consistently modified SN30000 sensitivity, even within a POR-negative background. Knockdown or genetic knockout of *POR* reduced SN30000 reductive metabolism and clonogenic cell death and similarly reduced sensitivity to TH-302 under hypoxia. A retrospective evaluation of head and neck squamous cell carcinomas showed heterogeneous POR expression and suggested a possible relationship between human papillomavirus status and HAP sensitivity. Taken together, our study identifies POR as a potential predictive biomarker of HAP sensitivity that should be explored during the clinical development of SN30000, TH-302, and other hypoxia-directed agents. *Cancer Res; 75(19); 4211–23. ©2015 AACR.*

Introduction

Hypoxia is a prevalent feature of the tumor microenvironment that has been implicated in neoplastic progression (1), dissemination (2) and resistance to ionizing radiation (3). Reflecting these effects, hypoxia has been compellingly linked to adverse outcome in malignancies for which radiotherapy is administered with curative intent (4), and agents that target tumor hypoxia promise to improve outcomes in radiation oncology.

Hypoxia-activated prodrugs (HAP) have been developed to target hypoxic tissue (5). HAPs are metabolized, typically by flavoenzyme-catalyzed one-electron reduction, to a prodrug radical from which an active cytotoxin is subsequently derived (6). In the presence of oxygen, the radical is back-oxidized to the initial prodrug, and in this manner HAPs exploit hypoxia to achieve selectivity (6). The most advanced clinical agent in this class is the nitroimidazole mustard evofosfamide (TH-302; refs. 7, 8), which is in phase III trials for pancreatic adenocarcinoma and soft tissue sarcoma (NCT01746979 and NCT01440088).

The benzotriazine di-*N*-oxide tirapazamine (TPZ) is the most thoroughly studied HAP (9). Metabolic activation of TPZ releases free radicals that damage DNA (10) and selectively kill hypoxic cells (11). TPZ showed promising activity in early clinical studies (12, 13). However, the addition of TPZ to chemoradiotherapy for head and neck squamous cell carcinoma (HNSCC) failed to extend survival in a pivotal trial (14). This disappointing outcome has been attributed to poor compliance with radiotherapy protocols at some centers (15), differential impact of TPZ in HPV-positive and -negative tumors (16) and failure to select patients for presence of tumor hypoxia (17, 18). Moreover, TPZ shows poor tumor penetration (19–21), a liability that is corrected in the second-generation TPZ analogue SN30000 (Fig. 1A), which was

[1]Auckland Cancer Society Research Centre, Faculty of Medical and Health Sciences, University of Auckland, Auckland, New Zealand. [2]Research Division, Peter MacCallum Cancer Centre, East Melbourne, Victoria, Australia. [3]Sir Peter MacCallum Department of Oncology, University of Melbourne, Parkville, Victoria, Australia. [4]Princess Margaret Cancer Centre, University Health Network, Toronto, Ontario, Canada. [5]AnQual Laboratories, School of Pharmacy, Faculty of Medical and Health Sciences, University of Auckland, Auckland, New Zealand. [6]Department of Otolaryngology–Head and Neck Surgery, University of Toronto, Toronto, Ontario, Canada. [7]Department of Radiation Oncology, University of Toronto, Toronto, Ontario, Canada. [8]Donnelly Centre and Banting and Best Department of Medical Research, University of Toronto, Toronto, Ontario, Canada. [9]Institute of Medical Science, University of Toronto, Toronto, Ontario, Canada. [10]Department of Medical Oncology, Peter MacCallum Cancer Centre, East Melbourne, Victoria, Australia. [11]Department of Medical Biophysics, University of Toronto, Toronto, Ontario, Canada. [12]Ontario Institute for Cancer Research, Toronto, Ontario, Canada.

Note: Supplementary data for this article are available at Cancer Research Online (http://cancerres.aacrjournals.org/).

Corresponding Author: Bradly G. Wouters, Princess Margaret Cancer Research Tower, MaRS Centre, 12th Floor Room 12-401, 101 College Street, Toronto, ON, M5G 1L7, Canada. Phone: 416-581-7861; Fax: 416-946-2984; E-mail: bwouters@uhnresearch.ca

doi: 10.1158/0008-5472.CAN-15-1107

Published OnlineFirst August 21, 2015; DOI: 10.1158/0008-5472.CAN-15-1107

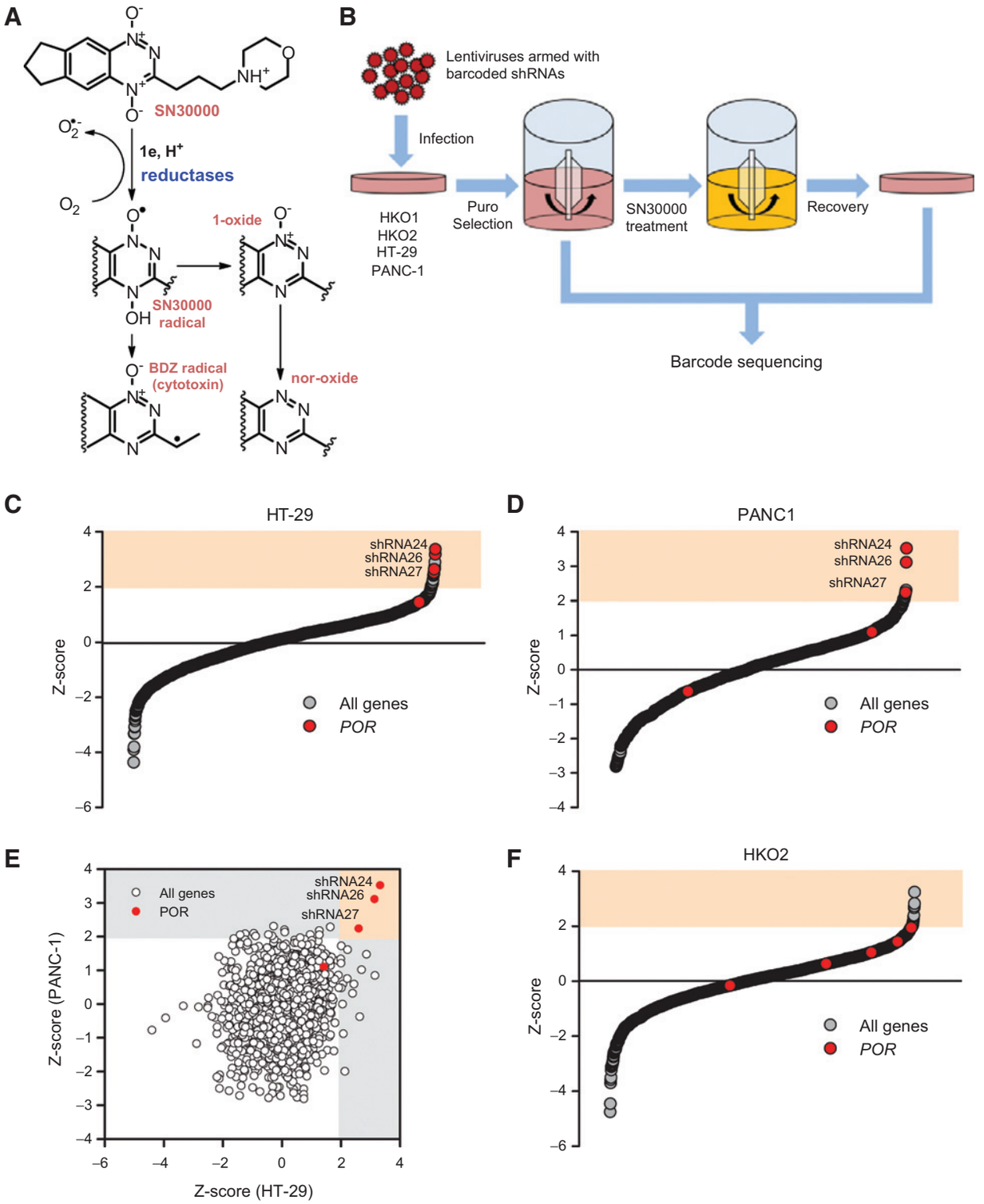

Figure 1.
High-throughput SN30000 reductase shRNA screens in carcinoma cell lines. A, chemical structure of the benzotriazine di-*N*-oxide HAP SN30000 and its reductive metabolism to the cytotoxic benzodiazinyl (BDZ) radical, as based on (27). B, schematic overview of the SN30000 screening workflow used in this study. C and D, waterfall plots of *Z*-scores for shRNA enrichment factors, arrayed by ascending magnitude of effect, for HT-29 and PANC-1. The colored fields indicate $Z > 1.96$. Data points corresponding to *POR*-targeted hairpins are highlighted in red with specific shRNAs labeled. E, scatter plot of *Z*-scores for all unique shRNAs in the HT-29 and PANC-1 reductase screens. Gray fields indicate $Z > 1.96$ for either line, with the red field indicating $Z > 1.96$ in both genetic backgrounds. As for B, *POR* hairpins are colored red with the three shRNA significantly selected in both cell lines labeled. F, waterfall plot of *Z*-scores for shRNA enrichment factors, arrayed by ascending magnitude of effect, for the HKO2 ($POR^{-/-}$) reductase screen.

Published OnlineFirst August 21, 2015; DOI: 10.1158/0008-5472.CAN-15-1107

developed using a lead selection algorithm that explicitly considered extravascular transport (21, 22). These agents are equivalent in mechanism of action (22–24) and nonclinical toxicology (22); however, SN30000 provides superior plasma pharmacokinetics in rodents, shows faster diffusion through three-dimensional cell cultures and is more active in multiple xenografts (22).

Experience with this therapeutic class suggests that selecting tumors that express the intended target is essential for optimizing their clinical use. However, biomarkers of sensitivity to HAPs are poorly defined and this remains a major challenge in patient stratification. Prior studies have focused on known aspects of HAP pharmacology, such as hypoxia (17), and the role of DNA-damage responses (10, 23, 25, 26). Reductive activation is also a requirement for HAP effect; however, the identity of enzymes that activate HAPs, their potential as sensitivity biomarkers, and variation of their expression in tumors has not been resolved.

Here, we use functional genetic screens to identify genes that are required for sensitivity to the HAP SN30000 under hypoxia in three genetically diverse cancer cell lines. This HAP confers a technical advantage, as the active cytotoxin is an oxidizing free radical (27) that is likely to be cell-entrapped. This lack of a bystander effect ensures that sensitivity is cell-autonomous—a requirement for pooled shRNA screens that is met by SN30000 under the conditions used. Barcoded lentiviral shRNA libraries were deployed to detect shRNAs that confer HAP resistance under hypoxia (i.e., sensitivity genes). Surprisingly, only one gene is consistently identified, namely the flavoprotein P450 oxidoreductase (*POR*). Immunohistochemistry for POR in HNSCC showed a wide range of staining intensities. A subset of cases showed evidence of both hypoxia and extensive POR expression. This study identifies POR as the principal determinant of sensitivity to SN30000 that should be explored as a predictive marker in the clinical development of this and other HAPs.

Materials and Methods

Compounds

SN30000 (22), TH-302 (28) and F-MISO (29) were synthesized at the Auckland Cancer Society Research Centre as reported. Octadeuterated SN30000 and its 1-oxide and nor-oxide metabolites were prepared as previously (24). DPI was purchased from Sigma-Aldrich.

Cell lines

HCT116, HT-29, PANC-1, and HEK293T cells were obtained from suppliers and cultured in media per Supplementary Table S1. Establishment of HCT116 clones with heterozygous or homozygous deletion of *POR*, designated HKO1 and HKO2, respectively, is reported elsewhere (30). HCT116 cells with varying levels of forced expression of POR were cloned from a previously reported pool (31). We isolated 11 clones and screened for one-electron reductase activity using the fluorogenic probe FSL-61 (EnSpire 2300 plate reader; Perkin Elmer; excitation/emission wavelengths 355/460 nm; ref. 32), using sulforhodamine B colorimetry to normalize for cell density. Eight clones spanning the greatest range of normalized FSL-61 activation were carried forward. Expression of *POR* mRNA in these clones was characterized by quantitative real-time PCR as described in Supplementary Methods. HCT116 cells carrying a neomycin resistance marker were obtained from Dr. A. Patterson (University of Auckland, Auckland, New Zealand). All cell lines were propagated for <2 months cumulative passage from frozen stocks confirmed to be *Mycoplasma*-free by PCR-ELISA (Roche Diagnostics). Cell lines were authenticated by commercial suppliers (HCT116, PANC-1, HEK293T) or by short tandem repeat (STR) profiling (HT-29).

High-throughput shRNA screens

As a screening library, we used the Sigma MISSION TRC1 lentiviral shRNA pool, which encompasses 82,017 barcoded shRNAs targeting 16,019 genes (33). Generation of a custom "reductase" library of 1,821 shRNAs covering 359 genes, including the majority of annotated human flavoproteins, is described in Supplementary Methods. We designed pharmacologically relevant shRNA screens using SN30000 exposures consistent with plasma pharmacokinetics achieved below murine MTD (22). Screens were calibrated to robustly detect (Z-scores > 1.96) hairpins that conferred resistance to SN30000 with dose-modifying factors greater than approximately 1.2. Cell lines were transduced using a nominal multiplicity of infection (MOI) of 0.3 and mean clonal representation of >2,000 (whole-genome) or >11,000 transduced cells/shRNA (reductase screens). Transduced cultures were selected in puromycin (3 μmol/L for HT-29, HKO1, and HKO2; 8 μmol/L for PANC-1) 24 hours after infection for 2 to 3 days. After recovering stably transduced cells, pretreatment samples (3×10^7 cells) were banked at −80°C for barcode sequencing. Single-cell suspensions (10^6/mL in MEMα + 10% FCS equilibrated to anoxic conditions for >3 days) containing 7.5×10^7 (reductase screens) or 2×10^8 (whole-genome screens) cells in polystyrene spinner flasks (Corning) were depleted of oxygen for 30 minutes inside a Whitley A85 Workstation (Don Whitley Scientific; <10 ppm O_2) and then exposed to SN30000 (30 μmol/L, HKO1; 25 μmol/L, HKO2; 14 μmol/L, PANC-1 and HT-29) for 1 hour under anoxia. The cells were then reoxygenated, SN30000 removed by centrifugation and the cultures maintained under conventional adherent conditions until regrown to the original population size with no further cell death apparent by phase-contrast microscopy (typically ∼2 weeks), at which time posttreatment samples (3×10^7 cells) were banked at −80°C for analysis. Single cells were plated out immediately prior to and following drug treatment, and at endpoint, to measure plating efficiency and surviving fraction.

Biologic samples were split into two to three technical replicates and genomic DNA was extracted using a QIAamp DNA Blood Maxi Kit (Qiagen) with an additional ethanol precipitation step. Barcode-containing cassettes were PCR amplified, using *Ex Taq* DNA polymerase (Takara Bio), for 33 reaction cycles using one universal primer and a pool of unique barcoded primers (one per DNA sample to enable multiplexed sequencing; Supplementary Table S2). The amplicons were resolved using Novex TBE gels (Life Technologies) and extracted using a digestion and purification kit (Qiagen). The isolated product was then deep sequenced using an Illumina HiSeq2000, with the first read being a single-end 50 base pair read from the TRC1/TRC2 sequencing primers and the second read a 6-base pair read from the barcode sequencing primer (Supplementary Table S2). FASTQ files were decompressed, the sequences trimmed, and aligned to an index using Bowtie (v.1). Sequencing depth was >1,500 mean mapped reads per shRNA. Read counts were normalized against the total number of mapped sample reads. The mean number of normalized reads between two and three technical replicates was calculated for each sample. Any shRNAs with unacceptably low representation (<5 normalized reads) were excluded from subsequent analysis. The

Published OnlineFirst August 21, 2015; DOI: 10.1158/0008-5472.CAN-15-1107

enrichment factor for shRNAs was defined as (mean posttreatment normalized reads/mean pretreatment normalized reads). We computed the $\log_2$ of these quotients then performed *Z*-transformation. Hairpins enriched above a *Z*-score of 1.96 were considered to be statistically significant.

Cytotoxicity assays

The sensitivity of cell lines to HAPs was evaluated by clonogenic survival. Shaking single-cell suspensions (10^6 cells in 1 mL anoxic MEMα + 10% FCS; Eppendorf Thermomixer) were preincubated under anoxic conditions for 30 minutes before exposing to prodrugs (concentrations specified in figure legends) for 1 hour, thus recapitulating the conditions used for shRNA screens. For DPI treatment, cells were exposed to 100 μmol/L DPI throughout preincubation and drug treatment. Colonies were scored after 10 days (HCT116, HKO1, and HKO2), 14 days (HT-29), or 21 days (PANC-1), with two to three replicates per condition per experiment.

Western blotting

Protocols for Western immunoblotting are described in Supplementary Methods.

RNA interference

Plasmids encoding four *POR*-targeting shRNAs represented on the TRC1 library: TRCN0000046523, TRCN0000046524, TRCN0000046526, and TRCN0000046527, in addition to empty pLKO.1 vector, were purchased from Sigma-Aldrich. The plasmids were packaged into lentiviruses and HCT116, HKO1, HT-29, and PANC-1 cells infected at an MOI of 0.3, with puromycin selection (4–8 μg/mL) administered for 72 hours. Transduced pools were maintained in 4 μg/mL puromycin. Knockdown efficacy was evaluated by Western immunoblotting and relative quantification of *POR* mRNA, using *ACTB* as a reference, by real-time PCR using primer sequences listed in Supplementary Table S3.

Targeted proteomics

Quantitation of POR protein by targeted proteomics was performed as described in Supplementary Methods.

SN30000 metabolism assays

Metabolic reduction of SN30000 to the corresponding 1-oxide and nor-oxide in anoxic cells was measured using a validated liquid chromatography–tandem mass spectrometry assay as described previously (24). Prodrug exposure conditions were as before, except that a single SN30000 concentration of 30 μmol/L was used.

Immunohistochemistry

Details of ethical approval of tissue banking and analysis are provided in Supplementary Methods. FFPE whole-tissue sections or TMAs were incubated at 60°C for 30 minutes then dewaxed through xylenes and alcohols to water. Slides were then placed in Dako Target Retrieval Solution into a pressure cooker at 125°C and 17 PSA for 3 minutes before cooling to 90°C. Slides were then rinsed with H_2O and loaded onto an autostainer (Dako) that performed the following steps: 10 minutes in H_2O_2, 1 hour in primary antibody (1:500 dilution; mouse monoclonal sc25263, Santa Cruz Biotechnology, which has been validated for POR IHC; ref. 31), 1 hour in secondary antibody/detection with EnVision+ anti-mouse (Dako) and color development with diaminobenzidine chromogen (Dako). Slides were then counterstained with hematoxylin and mounted. Three tumors from each isogenic xenograft model (HKO1, HCT116 wild-type, and HCT116-POR) were used as controls as they showed nil, weak, and strong staining. CA-IX IHC used the mouse monoclonal antibody M75 (Dr. A. Harris, University of Oxford, Oxford, United Kingdom) as described previously (34). Intensity of staining for POR or CA-IX within the cell membrane and cytoplasm was scored by a single investigator (R.J. Young) as follows: 0 (none), 1 (weak), 2 (moderate), 3 (strong), and the proportion of cells with each level of intensity scored as a percentage. Histology scores (*H* scores) were defined as: (percentage of cells with intensity 1 staining × 1) + (percentage of cells with intensity 2 staining × 2) + (percentage of cells with intensity 3 staining × 3), giving a possible range of 0 to 300.

F-MISO metabolism assay

Reductive metabolism of F-MISO in hypoxic cells was assayed as described in Supplementary Methods.

Statistical analysis

Mean values are represented as bars in graphs; error bars signify SEM. Statistical tests are specified in figure legends and were performed using SigmaPlot v12.5 (Systat Software). *, $P < 0.05$; **, $P < 0.01$; ***, $P < 0.001$.

Results

Reductase-focused shRNA screens

Expression of prodrug-activating reductases is necessary for the antitumor activity of HAPs. To identify enzymes that activate HAPs, we constructed a custom "reductase" library of 1,821 shRNAs against 359 flavoproteins, oxidoreductases, and other genes of interest (see Supplementary Table S4 for a complete list). We designed high-throughput shRNA screens based on positive selection of HT-29 and PANC-1 cells exposed to SN30000 under severely hypoxic conditions (<10 ppm gas-phase O_2; Fig. 1B). We used a single cycle of short-term (1 hour) SN30000 treatment in stirred single-cell suspensions (10^6 per mL)—conditions found to minimize bystander cell killing (Supplementary Fig. S1). The dimensions of these screens were calibrated to allow for maximal analytic resolution while minimizing stochastic dropout of hairpins as a result of excessive cell killing. To determine optimal prodrug exposures, cells were treated with SN30000 and assayed for clonogenic survival (Supplementary Fig. S2). Prodrug treatments in the shRNA screens produced surviving fractions of 0.1 and 0.002 in these cell lines (Supplementary Table S5), with plating efficiency fully restored in cultures sampled at endpoint (Supplementary Fig. S3). Analysis of read count densities and unsupervised hierarchical clustering of Pearson correlations indicated that barcode sequencing was highly reproducible (Supplementary Fig. S4). Comparison of shRNA representation in pre- and posttreatment samples by deep sequencing of barcodes identified 25 hairpins that were significantly enriched in HT-29 cells while 16 shRNAs were enriched in PANC-1 (Table 1). A single shRNA against the flavoreductase *POR* was the most highly enriched construct in both cell lines, with four hairpins against *POR* enriched above 1.96 standard deviations in HT-29 and three hairpins in PANC-1 (Fig. 1C and D). Strikingly, the rank of *POR* shRNAs according to magnitude of effect was identical in HT-29

Published OnlineFirst August 21, 2015; DOI: 10.1158/0008-5472.CAN-15-1107

Table 1. All shRNA clones significantly enriched (Z > 1.96) in HT-29, PANC-1, and HKO2 reductase screens

HT-29				PANC-1				HKO2			
Gene	**shRNA**	**Enrichment**	***Z*-score**	**Gene**	**shRNA**	**Enrichment**	***Z*-score**	**Gene**	**shRNA**	**Enrichment**	***Z*-score**
POR	046524	9.43	3.34	*POR*	046524	55.06	3.50	*KDSR*	064864	9.73	3.21
UQCRQ	064272	8.21	3.17	*POR*	046526	30.79	3.10	*EHHADH*	365079	6.99	2.80
POR	046526	8.14	3.15	*ZNF618*	437785	9.68	2.29	*FNDC3B*	229811	6.44	2.70
CYB5R3	236409	6.54	2.88	*IQCF3*	257512	9.36	2.26	*PTGIS*	442248	6.18	2.65
PIP5K1A	199304	5.76	2.71	*POR*	046527	8.80	2.22	*PLOD3*	294012	4.96	2.37
CD160	417480	5.49	2.65	*SLC34A2*	427282	8.35	2.18	*TECRL*	158841	4.76	2.32
NDUFV3	220913	5.38	2.63	*TGM2*	000243	8.06	2.16	*HNRNPA0*	017236	4.51	2.25
POR	046527	5.34	2.61	*GRID2*	429619	7.49	2.11	*PYCR1*	038982	4.22	2.17
POR	046525	4.90	2.51	*TLL2*	432474	7.16	2.08	*GRID2*	063071	4.17	2.16
ELF4	013871	4.71	2.45	*DHCR24*	046508	7.01	2.06	*PRDX2*	064907	4.07	2.12
TXNRD3	246173	4.64	2.44	*ELAVL3*	063728	6.79	2.04	*UQCRH*	437224	3.94	2.08
RER1	157448	4.55	2.41	*LCE1E*	427812	6.77	2.04	*FAM76A*	128470	3.72	2.01
NDUFS2	307301	4.45	2.38	*SDR42E1*	432328	6.69	2.03	*ACOXL*	046150	3.69	2.00
DHRS1	219058	3.98	2.24	*CPA2*	371827	6.68	2.03	*PECR*	046540	3.62	1.98
CYP3A43	435039	3.96	2.23	*MIOX*	418687	6.41	2.00	*MTRR*	433695	3.58	1.96
TOR1AIP1	167883	3.94	2.23	*UQCRH*	437224	6.33	1.99	*PYCRL*	000340	3.57	1.96
FA2H	148962	3.71	2.15								
SRXN1	415883	3.57	2.10								
TECRL	159663	3.54	2.09								
CYP7A1	064258	3.51	2.08								
P4HA2	061995	3.48	2.07								
PRDX4	064819	3.37	2.03								
DUS4L	064856	3.37	2.03								
NDOR1	414256	3.34	2.02								
COL11A1	083375	3.32	2.01								

NOTE: For brevity, the common prefix "TCRN0000" has been removed from shRNA clone identifiers.

and PANC-1 (Fig. 1E; TCRN0000046524 > TCRN0000046526 > TCRN0000046527; henceforth shRNA 24, 26, 27 for brevity). To confirm that enrichment of hairpins against *POR* was an on-target effect, we screened an HCT116 clone (HKO2, HCT116-POR$^{-/-}$) in which both *POR* alleles were knocked out by frameshifting indels using custom-designed zinc finger nucleases (30). As expected, representation of *POR* shRNAs was unaffected by SN30000 treatment in HKO2 (Fig. 1F). Interestingly, no gene other than *POR* showed enrichment of >1 discrete hairpin in any cell line, including HKO2 (Supplementary Fig. S5), in which 16 hairpins against different targets were enriched (Table 1).

Validation of POR as a determinant of HAP sensitivity

Individual hairpins against *POR* were validated by transducing HT-29 and PANC-1 with pure lentiviruses carrying the two most strongly selected shRNAs, 24 or 26, in addition to the empty pLKO.1 vector. Expression of shRNA 24 or 26 suppressed POR protein in both cell lines whereas pLKO.1 had no effect (Fig. 2A and Supplementary Fig. S6). *POR* knockdown significantly increased clonogenic survival of HT-29 and PANC-1 cells exposed to SN30000 under hypoxia (Fig. 2B and Supplementary Fig. S7). A concomitant 75% loss of metabolic reduction of SN30000 to the corresponding 1-oxide and nor-oxide metabolites (Fig. 1A) was observed in transduced PANC-1 cells, with 43% loss of SN30000 activation seen in HT-29 (Fig. 2C). The single construct evaluated in this context, shRNA 24, also conferred resistance to the clinical prodrug TH-302 in PANC-1 cells, with 15-fold greater clonogenic survival at the highest prodrug concentration tested (Fig. 2D). We found expression of *POR* mRNA to correlate strongly with reductive metabolism of SN30000 and the closely related prodrug TPZ in a panel of 14 diverse carcinoma lines under hypoxia (Fig. 2E), suggesting this reductase to be generically central to enzymatic activation of these HAPs. Indeed, expression of *POR* showed the strongest correlation with activation of both SN30000 and TPZ among a survey of mRNAs corresponding to the entire annotated human flavoproteome (Supplementary Tables S6 and S7). The correlations were parsimonious with a linear dependence of HAP activation on *POR* abundance and predicted residual, POR-independent activation when the latter was extrapolated to zero expression.

Genome-wide shRNA screens

To identify determinants of sensitivity to SN30000 not solely related to reductive activation, we used the TRC1 whole-genome shRNA library to screen HCT116 clones in which single (HKO1, HCT116$^{+/-}$) or both (HKO2, HCT116-POR$^{-/-}$) *POR* alleles were inactivated (30). HKO1 and HKO2 cells were stably transduced with lentiviruses at an empirical MOI of 0.38 and 0.25, respectively and exposed to SN30000, after which surviving fractions were 0.008 and 0.1 (Supplementary Table S5). The treated cell populations were maintained until plating efficiency had returned to baseline levels (Supplementary Fig. S8). Barcode analysis in posttreatment cultures revealed 528 shRNAs significantly overrepresented ($Z > 1.96$) in HKO1 (Fig. 3A) and 1,967 in HKO2 (Fig. 3B and Supplementary Tables S8 and S9 for complete gene lists). A hairpin specific to *POR*, shRNA 24, was the most highly selected construct in HKO1 (35-fold increased representation; $Z = 4.2$; Fig. 3A). Two additional shRNAs specific to *POR*, shRNAs 26 and 27, also caused resistance to SN30000 in HKO1 (10- and 5-fold enrichment, respectively). This ranking of *POR* shRNAs was identical to that seen in HT-29 and PANC-1. In contrast, representation *POR* shRNAs was unaffected by SN30000 treatment in HKO2 (Fig. 3B). Strikingly, no targets other than *POR* were consistently selected in either HKO1 or HKO2; single shRNAs to six genes (*XAB2*, *AGAP3*, *FAM3A*, *ATP2A3*, *ITGB5*, and *SNTA1*) were enriched in both cell lines but none of the other three to four shRNAs to any of these targets conferred SN30000 resistance, suggesting these to be false positives of the type

Published OnlineFirst August 21, 2015; DOI: 10.1158/0008-5472.CAN-15-1107

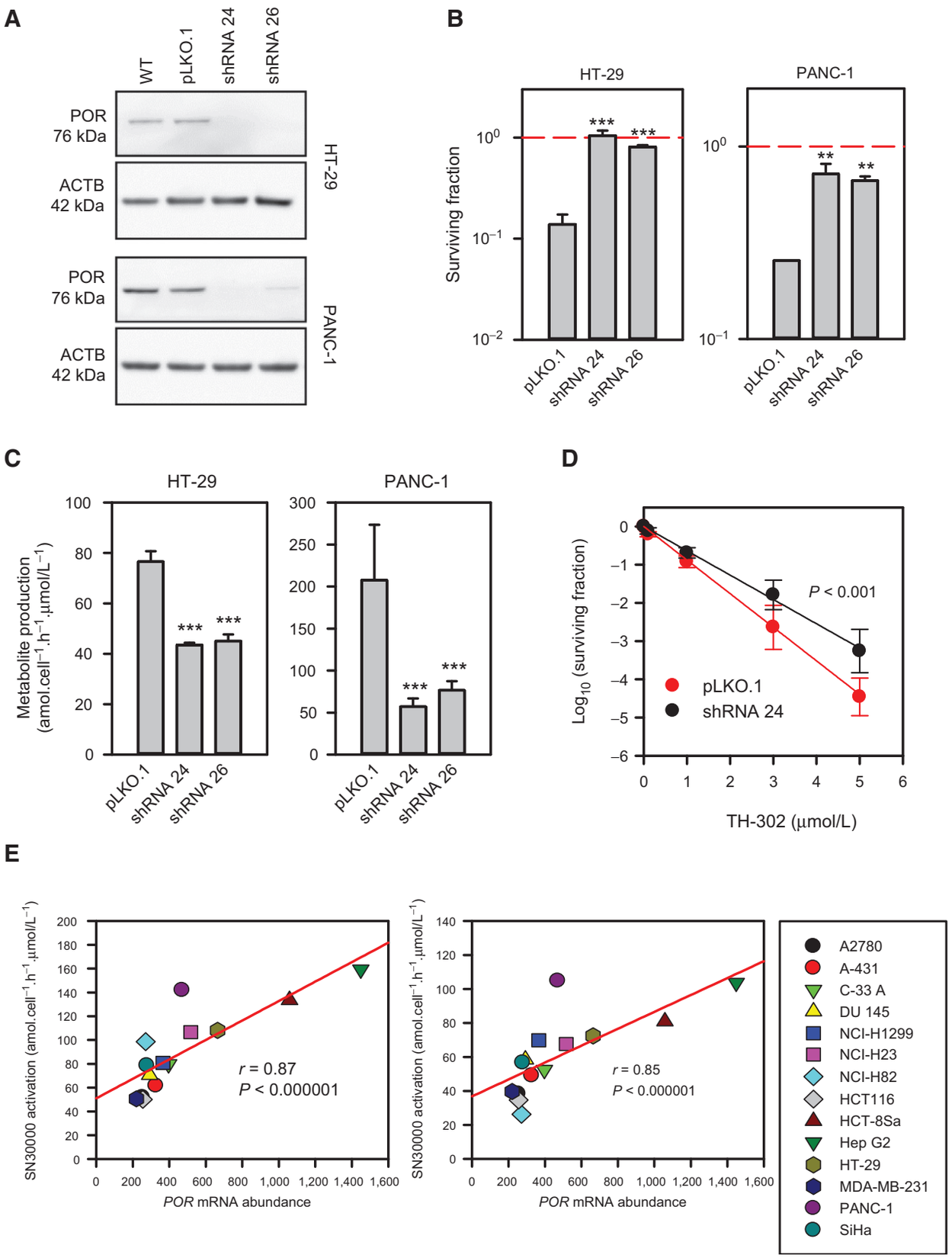

Published OnlineFirst August 21, 2015; DOI: 10.1158/0008-5472.CAN-15-1107

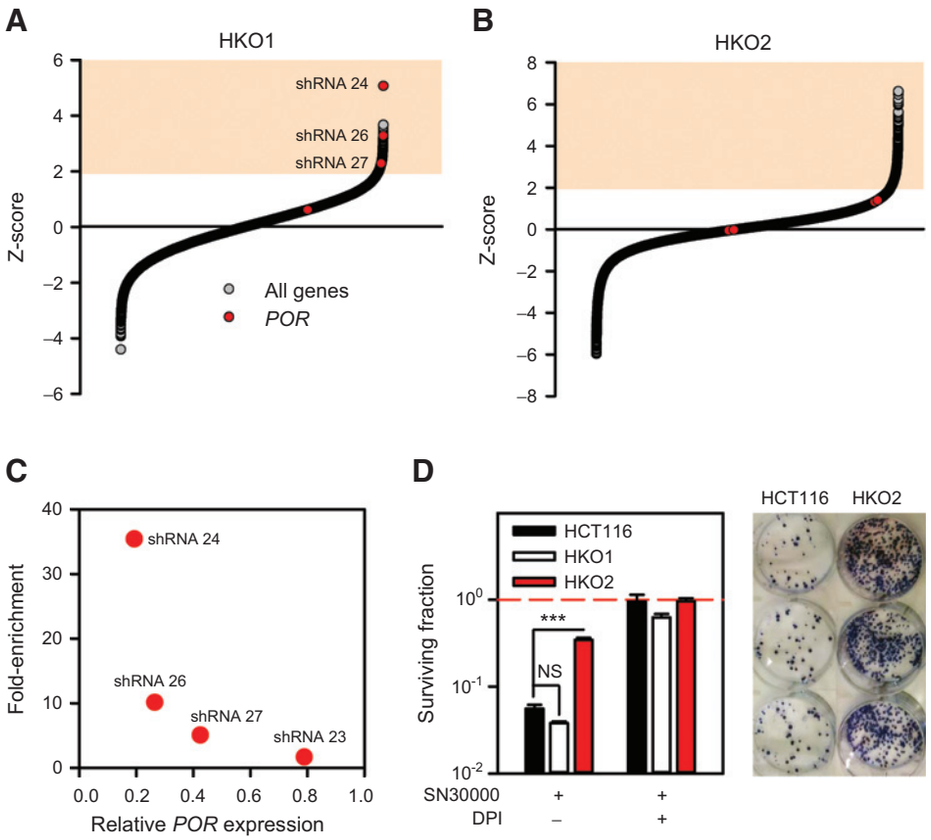

Figure 3.
Whole-genome lentiviral shRNA screens in *POR* hetero- and homozygous knockout cell lines. A and B, waterfall plots of *Z*-scores for shRNA enrichment factors (mean posttreatment normalized reads/mean pretreatment normalized reads), arrayed on the basis of magnitude of effect, for HKO1 ($POR^{+/-}$; A) and HKO2 ($POR^{-/-}$; B) whole-genome screens. The colored fields indicate significant enrichment ($Z > 1.96$). Data points corresponding to *POR*-targeted hairpins that are represented in the TRC1 library are colored in red. C, *POR* expression, relative to nontransduced cells, in HKO1 stably transduced with shRNAs against *POR* as a function of the enrichment factors for the same hairpins in the HKO1 whole-genome screen. D, clonogenic survival of HCT116, HKO1, and HKO2 cells treated with 25 μmol/L SN30000, for 1 hour under hypoxic conditions, in the presence or absence of the *pan*-flavoprotein inhibitor DPI (100 μmol/L, added 30 minutes before SN30000). The values are means and range of two cultures within a single experiment. Statistical significance of difference from HCT116 was evaluated using two-way ANOVA, with cell line and drug treatment as factors. The figure is representative of three separate experiments performed; these replicates are provided in Supplementary Fig. S10C. Two-way ANOVA using cell line and experiment number as factors similarly confirmed significant loss of SN30000 cytotoxicity in HKO2 across the three replicates. A representative photograph of methylene blue-stained colonies is shown. These HCT116 and HKO2 cells were exposed to SN30000 in the absence of DPI and 10^3 cells seeded in each well.

frequently observed in RNAi screens (35). No targets other than *POR* were significantly selected in any two of the three *POR*-proficient genetic backgrounds (Supplementary Fig. S9). There was also no overlap in the sets of hairpins enriched in the reductase-focused and genome-scale screens in HKO2.

We characterized *POR* knockdown in HKO1 cells stably transduced with four *POR* hairpins represented on the TRC1 library. Three constructs significantly antagonized *POR* expression, while pLKO.1 and the fourth *POR* hairpin, shRNA 23, had no effect (Supplementary Fig. S10A). There was an inverse monotonic

Figure 2.
Validation of *POR* shRNAs and effects on HAP metabolism and cytotoxicity. A, confirmation of POR knockdown by Western blotting in HT-29 and PANC-1 cells stably transduced with the two most strongly selected shRNAs against *POR*—shRNA 24 and 26. The blot shown is representative of three generated; these replicates and quantification thereof are provided in Supplementary Fig. S6. B, clonogenic survival of HT-29 and PANC-1 cells stably transduced with empty pLKO.1 or shRNAs 24 or 26 and exposed to SN30000, at 14 μmol/L, for 1 hour under hypoxic conditions. The values are means and SEM of three cultures within a single experiment that is representative of three assays performed. These replicates are provided in Supplementary Fig. S7. C, metabolic activation of SN30000 under hypoxic conditions in HT-29 and PANC-1 cells stably transduced with empty pLKO.1 or shRNAs 24 or 26. The values are interexperiment means and SEM of net metabolite production (i.e., 1-oxide plus nor-oxide) from three assays performed. Statistical significance in B and C was evaluated using one-way ANOVA. D, Spearman correlations of *POR* mRNA abundance, measured using Affymetrix Human Genome U133 Plus 2.0 arrays (44), with reductive metabolism of SN30000 and TPZ in a panel of 14 human carcinoma cell lines under hypoxia. Generation of the latter data sets has been described previously (24). E, clonogenic survival curves of PANC-1 cells stably transduced with empty pLKO.1 or shRNA 24 and exposed to TH-302 for 1 hour under hypoxic conditions. The values are interexperiment means and SEM from three assays performed. Statistical significance in differences in dose–response was evaluated by linear regression of the $\log_{10}$ of plating efficiency.

Published OnlineFirst August 21, 2015; DOI: 10.1158/0008-5472.CAN-15-1107

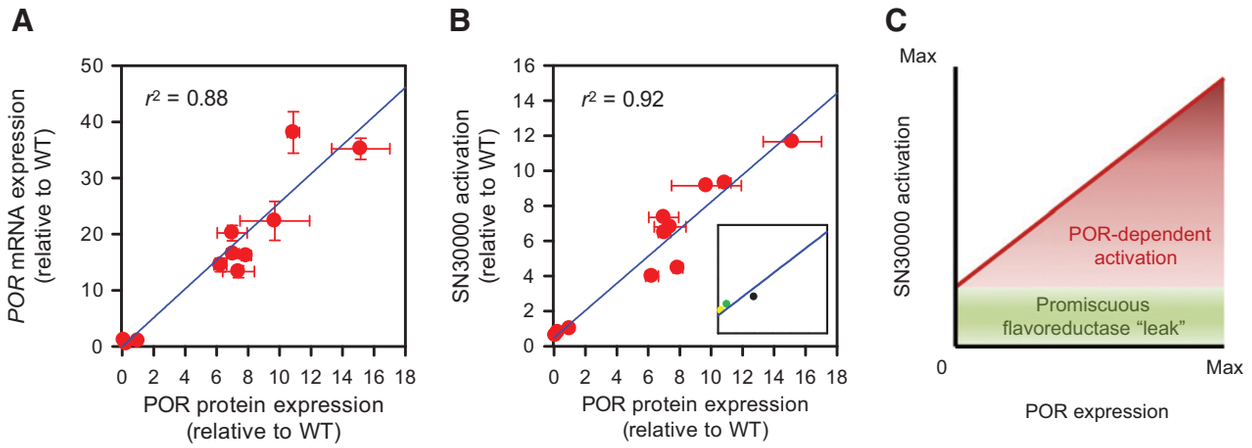

Figure 4.
Metabolic activation of SN30000 as a function of POR protein expression in an isogenic background. A, Pearson correlation of *POR* mRNA expression, measured by qPCR, and POR protein expression, measured by proteotypic peptide mass spectrometry in a panel of HCT116 clones with stable forced expression or knockout of *POR*. B, Pearson correlation of POR protein expression with metabolic activation of SN30000 under hypoxia in the same cell line panel. Inset, enlargement of the *y*-intercept illustrating the predicted residual SN30000 activation at extrapolation to zero POR expression; black, HCT116 wild-type; green, HKO1; yellow, HKO2. Values in A and B are intraexperiment means and SEM of three determinations. All three metrics are expressed as fold change relative to HCT116 wild-type. C, proposed "two component" model of SN30000 activation based on this study.

relationship between remaining *POR* mRNA in transduced HKO1 cells and degree of shRNA enrichment in the corresponding screen (Fig. 3C). The two most potent of these hairpins, shRNAs 24 and 26, were confirmed to deplete POR protein by immunoblotting of parental HCT116 cells (Supplementary Fig. S10B).

We next compared clonogenic survival of HKO2, HKO1 and wild-type cells treated with SN30000 under hypoxia (Fig. 3D and Supplementary Fig. S10C). HKO1 cells were equivalently sensitive to SN30000 as wild-type, whereas homozygous deletion of *POR* resulted in marked (two-way ANOVA, HKO2 vs. wild-type; $P < 0.001$) but incomplete (HKO2 treated vs. untreated; $P < 0.001$) suppression of cytotoxicity. Treatment with the *pan*-flavoprotein inhibitor diphenyliodonium (DPI) fully abolished SN30000 cytotoxicity in all three of these lines, suggesting that the POR-independent component of SN30000 cytotoxicity is flavoreductase-mediated.

Correlative analysis of POR expression and SN30000 activation

To characterize further the relationship between SN30000 activation and *POR* expression, we evaluated an isogenic panel of 11 HCT116 derivatives including wild-type, HKO1, HKO2 and nine clones isolated from a pool stably transfected for expression of *POR*. *POR* mRNA abundance spanned a range extending to approximately 38-fold higher than wild-type (Fig. 4A), which was significantly greater than variability observed in a mixed panel of 23 human carcinoma lines (Fig. 2D). There was a strong correlation between abundance of POR protein (determined by a quantitative targeted proteomic assay) and *POR* mRNA expression, though the gradient of this regression was approximately 2.6 (i.e., 35% increase in POR protein per 100% increase in mRNA; Fig. 4A). There was a strong linear association between POR protein and reductive metabolism of SN30000 under hypoxia (Pearson correlation, $r^2 = 0.92$; $P > 0.00001$), with a 77% increase in prodrug activation per unit increase in POR expression, and no evidence for saturation at the highest levels of POR examined (Fig. 4B). This correlation predicted residual activation of SN30000, at approximately 50% of wild-type when extrapolated to zero POR. This estimate was consistent with the corresponding modeling in genetically diverse carcinoma cells (Fig. 2D). These data supported a central role for *POR* as the enzyme predominantly responsible for activation of SN30000, but also implied the existence of additional DPI-sensitive flavoreductases that collectively contribute to a residual component of SN30000 reduction (flavoreductase "leak"; Fig. 4C).

Clinical analyses

Radiotherapy for locally advanced HNSCC is the setting in which hypoxia has been most compellingly linked to treatment failure (4). Therefore, to evaluate POR expression in HNSCC, we performed IHC on three clinically annotated cohorts. The first cohort consisted of a tissue microarray (TMA) of 340 paired 0.6-mm cores from 170 cases of lingual SCC treated at the Princess

Table 2. Quantitation of POR IHC staining intensity in three HNSCC cohorts

				H score: *n* (%)		
Cohort	**Anatomic site**	**Format**	***N***	**0–49**	**50–149**	**150–300**
Princess Margaret	Lingus	TMA	202[a]	4 (2%)	157 (78%)	39 (19%)
Peter MacCallum #1	Larynx	TMA	113	85 (75%)	21 (19%)	7 (6%)
Peter MacCallum #2	Oropharynx	Whole sections	22	7 (32%)	9 (41%)	6 (27%)
	Larynx	Whole sections	3	—	3 (100%)	—
	Hypopharynx	Whole sections	2	—	1 (50%)	1 (50%)
	Oral cavity	Whole sections	1	—	1 (100%)	—
	Total		28	7 (25%)	14 (50%)	7 (25%)

[a]202 cores corresponding to 122 cases.

Published OnlineFirst August 21, 2015; DOI: 10.1158/0008-5472.CAN-15-1107

Margaret Cancer Centre (Toronto, ON, Canada). Of these, 202 cores corresponding to 122 cases were evaluable for IHC, with adjacent nonmalignant tissue available from 78 cases (116 cores). POR expression was detectable in 200 of 202 cores (99%), with significant variation in intensity (*H* score range 20–290; Table 2) that was markedly more heterogeneous than in normal tissue (Fig. 5A). The endogenous hypoxia marker carbonic anhydrase IX (CA-IX) was expressed in 53% of serial sections from tumor cores, with coexpression of POR and CA-IX observed in 60% (113 of 188) and significant spatial overlap apparent in the subset

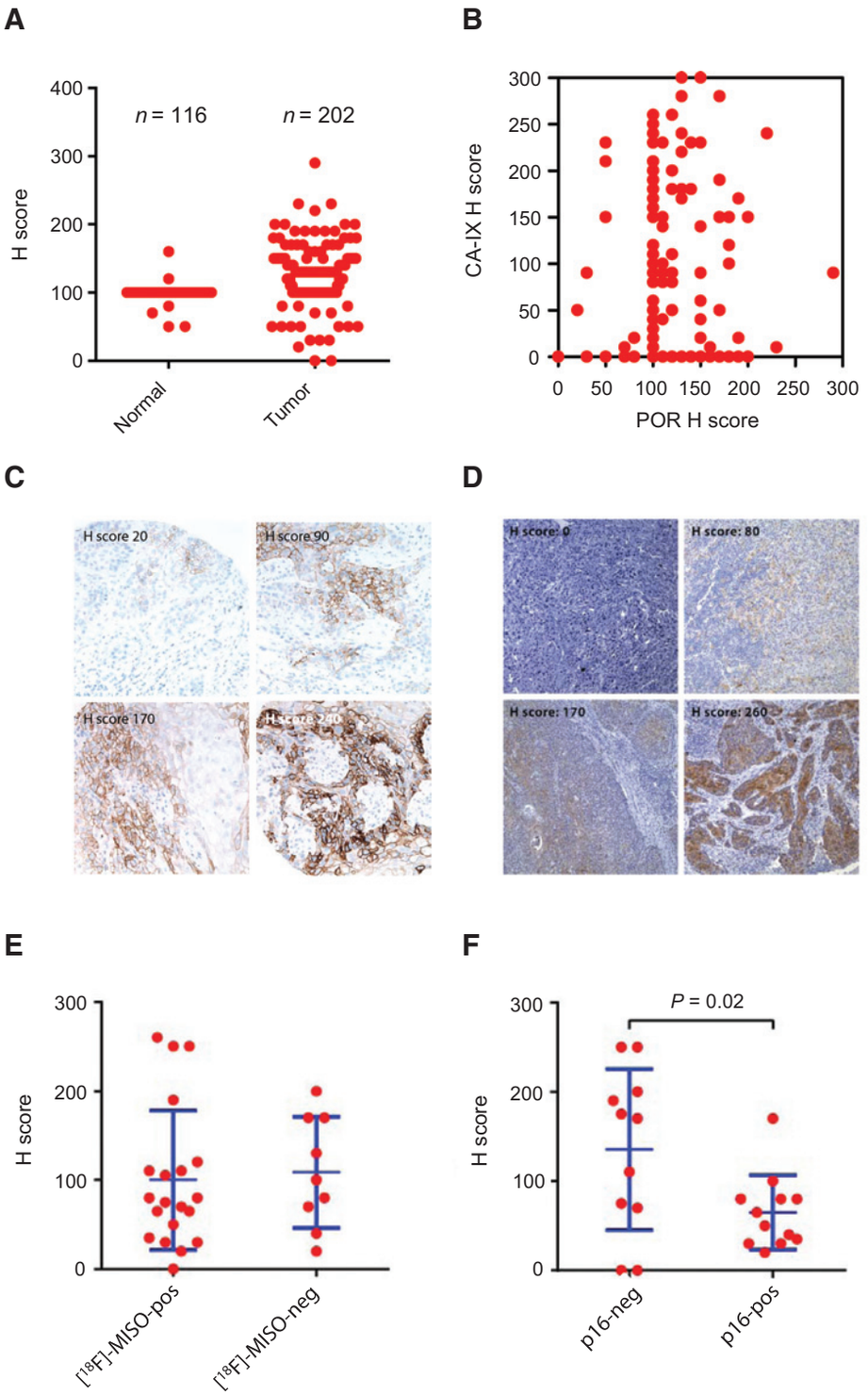

Figure 5.
Analysis of POR expression by IHC and hypoxia in HNSCC. A, comparison of POR H scores in lingual SCC cores and adjacent nonmalignant epithelia. B, coexpression of POR and the endogenous hypoxia marker CA-IX in lingual SCC cores. C, micrographs (×20 objective lens) showing CA-IX staining in representative lingual SCC cases from cohort 1. D, micrographs (×10 objective lens) showing POR staining in representative HNSCC cases from cohort 3. E, POR H scores according to tumor [^{18}F]-MISO PET status. F, HPV/p16 status in cohort 3. Statistical significance of differences in staining intensity between p16-positive/negative tumors was evaluated using unpaired *t*-tests.

Published OnlineFirst August 21, 2015; DOI: 10.1158/0008-5472.CAN-15-1107

evaluable for both antigens (Fig. 5B and Supplementary Fig. S11). Representative CA-IX staining in tumor tissue is shown in Fig. 5C. Minimal expression of CA-IX was detected in nonmalignant tissue (Supplementary Fig. S12A). POR staining was generally concordant between paired cores from individual tumors (linear regression $r^2 = 0.72$; Supplementary Fig. S12B), whereas poor agreement was seen in CA-IX staining (linear regression $r^2 = 0.39$; Supplementary Fig. S12C), emphasizing the challenge of core biopsy sampling of regionally heterogeneous hypoxia.

The second cohort consisted of 113 cases of laryngeal SCC treated at the Peter MacCallum Cancer Centre (Victoria, Australia). These were represented as single 1-mm cores on a TMA, with matched whole sections for 13 tumors. We observed a wide range of POR expression across the cohort (Table 2), which was lower than lingual SCC (Supplementary Fig. S12D). Of the 113 laryngeal SCC cores, 47 (42%) showed detectable POR, with an *H* score range of 10 to 270. There was poor concordance between POR staining intensity in TMA cores and matched whole sections (linear regression $r^2 = 0.49$; Supplementary Fig. S12E), presumably reflecting higher inter-core variability in POR *H* score than seen in the lingual SCC cohort (Supplementary Fig. S12D).

The third cohort comprised whole sections from 28 HNSCCs (22 oropharyngeal, 3 laryngeal, 2 hypopharyngeal, and 1 oral) from prior phase I and II trials of TPZ with chemoradiotherapy at the Peter MacCallum Cancer Centre (17, 36). These were annotated with HPV/p16 status and functional hypoxia imaging ([^{18}F]-MISO PET). We again observed a wide range of POR *H* scores (range 0–260; Table 2; Fig. 5D); 26 cases (93%) showed detectable expression, with intermediate (50–150) and intense expression (>150) observed in 50% and 25% of tumors, respectively. Notably, several tumors with intense POR staining were also classified as hypoxic by [^{18}F]-MISO PET (Fig. 5E and Supplementary Fig. S12F), confirming that a subset of patients present with disease expected to be highly sensitive to HAPs. Of interest, we observed significantly higher POR expression in HPV/p16-negative HNSCC (*H* score mean ± SEM: 136 ± 27) compared with HPV/p16-positive tumors (*H* score 65 ± 12; unpaired *t* test $P < 0.05$; Fig. 5F). Although this cohort was too small to robustly relate clinical outcome to the relevant variables (treatment, POR, hypoxia and HPV/p16), it was of interest that two of the four low-POR, hypoxic, HPV-negative tumors that received TPZ had locoregional recurrence, whereas the two high-POR tumors of the same type were 7 years disease-free and 3.3 years disease-free then distant relapse without recurrence within the radiation field. Notably, we showed that F-MISO is also a reductive substrate for POR (Supplementary Fig. S12G), suggesting that high-POR malignancies may produce greater hypoxia PET avidity as a result of facile tracer activation.

Within all three HNSCC cohorts the range in POR expression recapitulated that observed in preclinical models used in the discovery screens, including tumors cultivated from the HCT116 wild-type and *POR*-knockout lines (Supplementary Fig. S13). Indeed, three HCT116 xenografts scored for POR IHC showed *H* scores of 70, 90, and 100, suggesting that POR is likely to be a significant determinant of HAP activity at levels of expression comparable that observed in primary HNSCC. Our IHC data were also consistent with a comprehensive genomic analysis of 279 HNSCC recently published by The Cancer Genome Network, in which *POR* was mutated, with the majority of such alterations representing gene amplification, or transcriptionally upregulated (*Z*-score > 1.96) in 30 of 243 HPV-negative tumors (Supplementary Fig. S14), whereas no mutations and only one instance of mRNA upregulation was found among 36 HPV-positive cases (37).

Discussion

Variation in clinical responses to antineoplastic therapies is a long-standing challenge in the management of cancer. Despite a growing appreciation for the importance of this field (38, 39), genetic determinants of sensitivity to HAPs remain poorly understood. In addition to tumor hypoxia, which is the fundamental target of HAPs, expression of prodrug-activating reductases is reasoned to be a key determinant of response to bioreductive agents (5). Candidate-based approaches have identified a collection of flavoreductases capable of activating HAPs by one-electron (oxygen-sensitive) reduction, including POR (40–42), NDOR1 (31, 42, 43), MTRR (31, 42, 44), thioredoxin reductase (45), FOXRED2 (44), NOS2A (31, 42), and CYB5R3 (46). However, classification of these enzymes as HAP reductases has largely relied on studies with purified enzymes or forcing expression to supraphysiologic levels. Thus, the enzymology of HAP activation at endogenous levels of expression in human malignancy has been an ongoing area of uncertainty and is a barrier to optimizing the clinical use of these agents.

This study conclusively demonstrates POR to make the largest modifiable contribution to the activity of the benzotriazine di-*N*-oxide SN30000, which we used as a model HAP, in three different cancer cell lines under hypoxia. The functional genomic data and hairpin validation are strikingly consistent, with complete concordance between *POR* knockdown efficiency and enrichment of constructs in the screens. Importantly, *POR* was found to be a major determinant of SN30000 activity in HKO1 cells despite low levels of expression in this line (POR protein abundance 26% of HCT116 wild-type). This finding challenges previous assessments that modest expression of POR in human tumor cores (31) and xenografts (47) may limit its utility as a predictive biomarker. Indeed a significant fraction of cases within our three HNSCC cohorts showed markedly more intense POR staining than HCT116 xenografts (Fig. 5 and Supplementary Fig. S11–S13), which are sensitive to SN30000 (24), suggesting that POR will contribute significantly to HAP activity in a defined subset of patients.

Our data are also consistent with a second, POR-independent component to SN30000 activity that is sensitive to DPI inhibition (thus flavoenzyme-mediated; Fig. 3D). Linear regression of *POR* mRNA abundance with SN30000 metabolism in a panel of cancer cell lines (Fig. 2D) suggests this component to be ubiquitous across diverse genetic backgrounds. A surprising finding of this study is that the genes responsible for this secondary component of prodrug activity were refractory to identification by shRNA screening. No shRNA targets consistently conferred resistance to SN30000 in *POR*-null HKO2 cells nor were any genes other than *POR* robustly enriched in PANC-1, HT-29, or HKO1. There are several plausible explanations for this finding. Genes essential for cell survival are inaccessible to positive-selection drug treatment screens. However, of the entire annotated human flavoproteome, only one gene (succinate dehydrogenase complex subunit A; *SDHA*) was found to be essential in a significant subset cancer cell lines screened with the TRC1 shRNA library, with dropout of this gene in 29 of 72 cell lines screened in the same laboratory (33). Furthermore, no flavoproteins were essential in HCT116 cells specifically, with only

two (sarcosine dehydrogenase; *SARDH* and mitochondrial tRNA translation optimization 1; *MTO1*) necessary for the viability of PANC-1 cells (33). Thus, we consider essentiality to be an unlikely explanation in this instance. A second possibility is an absence of efficient shRNA reagents against important non-*POR* targets in the TRC1 library. Although impossible to definitively reject, invoking false-negatives is unconvincing in light of the multiple, sequence-verified constructs against each target represented on the shRNA library. Moreover, our custom reductase library was deliberately composed to include hairpins for which prior characterization of knockdown efficacy was available. A more likely explanation is that the POR-independent component of SN30000 activation is highly promiscuous, with multiple flavoreductases contributing below the detection limit of our screens. Strategies to improve the analytic power of these experiments may, therefore, facilitate identification of the next layer of genetic determinants. Potential solutions include extending SN30000 selection over multiple cycles of prodrug treatment or using CRISPR/Cas9 screening platforms, which provide definitive genetic knockout phenotypes (50).

As a single gene apparently responsible for a major component of HAP activity, tumor expression of *POR* may be highly tractable as a predictive biomarker. At the time of our study, expression of POR in human tumors was not well described. The most extensive analysis presently reported in the literature found 21% of 685 cases represented on mixed and disease-specific TMAs to express detectable POR (31). However, low representation of malignancies considered to be priority indications in the context of HAP development, particularly HNSCC, arguably limited the translational utility of these data. Our more focused expression analysis described a wide range of POR staining intensities in HNSCC, with a significant fraction of cases found to express POR at levels consistent with a major contribution to SN30000 activity (Table 2). Importantly, a subset of these carcinomas were also classified as hypoxic by [^{18}F]-MISO imaging or CA-IX staining, confirming coincidence of these two targets (hypoxia and POR) in a defined population of patients. The observation that POR immunostaining shows much less intratumor heterogeneity compared with that of CA-IX is a major advantage for evaluating the expression of the former in tissue from core biopsy or surgical resection. Such an approach could complement imaging-based measures of tumor hypoxia, which may overcome the challenge of tissue sampling variability presented by the spatial heterogeneity of hypoxia. The trend toward higher POR expression in HPV-negative tumors requires confirmation in larger cohorts but is of interest as these malignancies are associated with poor prognosis and show the greatest response to HAPs (16).

With ongoing development of gene expression signatures and imaging modalities as biomarkers of tumor hypoxia in HNSCC (48, 49) POR could conceivably be integrated with these tests and routine HNSCC histopathology assays to support patient stratification in HAP development. Whether POR expression is predictive of HAP sensitivity in hypoxic tumors, and whether promiscuous "flavoreductase leak" affords sufficient prodrug activation for antineoplastic activity in the absence of POR, are priority questions that should be addressed in clinical evaluation of SN30000, TH-302 and other HAPs.

Disclosure of Potential Conflicts of Interest

D. Rischin is a consultant/advisory board member of Threshold. W.R. Wilson has ownership interest (including patents) in a patent inventorship. No potential conflicts of interest were disclosed by the other authors.

Authors' Contributions

Conception and design: F.W. Hunter, J. Moffat, M. Koritzinsky, W.R. Wilson, B.G. Wouters

Development of methodology: F.W. Hunter, R.J. Young, Y. Gu, W.R. Wilson, B.G. Wouters

Acquisition of data (provided animals, acquired and managed patients, provided facilities, etc.): F.W. Hunter, R.J. Young, Z. Shalev, R.N. Vellanki, J. Wang, Y. Gu, N. Joshi, S. Sreebhavan, I. Weinreb, D.P. Goldstein, T. Ketela, B. Solomon, D. Rischin, B.G. Wouters

Analysis and interpretation of data (e.g., statistical analysis, biostatistics, computational analysis): F.W. Hunter, R.J. Young, Z. Shalev, R.N. Vellanki, J. Wang, Y. Gu, N. Joshi, S. Sreebhavan, J. Moffat, K.R. Brown, B. Solomon, W.R. Wilson, B.G. Wouters

Writing, review, and/or revision of the manuscript: F.W. Hunter, R.J. Young, R.N. Vellanki, Y. Gu, I. Weinreb, D.P. Goldstein, B. Solomon, D. Rischin, W.R. Wilson, B.G. Wouters

Administrative, technical, or material support (i.e., reporting or organizing data, constructing databases): F.W. Hunter

Study supervision: D. Rischin, W.R. Wilson, B.G. Wouters

Other (performed a small part of the study): N. Joshi

Acknowledgments

The authors thank Dr. Michael Hay for synthesis of SN30000 and TH-302, Dr. Moana Tercel for synthesis of F-MISO, and the Head and Neck team led by Dr. Fei-Fei Liu at the Princess Margaret Cancer Centre for assistance with the provision of clinical samples.

Grant Support

This research was supported by Programme Grants 11/1103 and 14/538 from the Health Research Council of New Zealand, grants from the Ontario Ministry of Health and Long Term Care (OMOHLTC), the Terry Fox Research Institute (TFRI-PPG 1036), the Ontario Institute for Cancer Research, the Canadian Institute for Health Research (CIHR grant 201592), and a project grant from the National Health and Medical Research Council of Australia. F.W. Hunter is supported by grants from Genesis Oncology Trust (GOT-1438-JGPDF), Auckland Cancer Society (Brett Roche Memorial Award), and John Logan Campbell Medical Trust (Travel Grant). Y. Gu is supported by grants from the Marsden Fund (Fast Start 13/036) and Auckland Medical Research Foundation (1114005).

The costs of publication of this article were defrayed in part by the payment of page charges. This article must therefore be hereby marked *advertisement* in accordance with 18 U.S.C. Section 1734 solely to indicate this fact.

Received April 24, 2015; revised June 23, 2015; accepted July 15, 2015; published OnlineFirst August 21, 2015.

References

1. Höckel M, Schlenger K, Aral B, Mitze M, Schaffer U, Vaupel P. Association between tumor hypoxia and malignant progression in advanced cancer of the uterine cervix. Cancer Res 1996;56:4509–15.
2. Brizel DM, Scully SP, Harrelson JM, Layfield LJ, Bean JM, Prosnitz LR, et al. Tumor oxygenation predicts for the likelihood of distant metastases in human soft tissue sarcoma. Cancer Res 1996;56:941–3.
3. Wouters BG, Brown JM. Cells at intermediate oxygen levels can be more important than the "hypoxic fraction" in determining tumor response to fractionated radiotherapy. Radiat Res 1997;147:541–50.
4. Nordsmark M, Bentzen SM, Rudat V, Brizel D, Lartigau E, Stadler P, et al. Prognostic value of tumor oxygenation in 397 head and neck tumors after

primary radiation therapy. An international multi-center study. Radiother Oncol 2005;77:18–24.
5. Wilson WR, Hay MP. Targeting hypoxia in cancer therapy. Nat Rev Cancer 2011;11:393–410.
6. Wardman P, Dennis MF, Everett SA, Patel KB, Stratford MR, Tracy M. Radicals from one-electron reduction of nitro compounds, aromatic N-oxides and quinones: the kinetic basis for hypoxia-selective, bioreductive drugs. Biochem Soc Symp 1995;61:171–94.
7. Chawla SP, Cranmer LD, Van Tine BA, Reed DR, Okuno SH, Butrynski JE, et al. Phase II study of the safety and antitumor activity of the hypoxia-activated prodrug TH-302 in combination with doxorubicin in patients with advanced soft tissue sarcoma. J Clin Oncol 2014;32:3299–306.
8. Borad MJ, Reddy SG, Bahary N, Uronis HE, Sigal D, Cohn AL, et al. Randomized phase II trial of gemcitabine plus TH-302 versus gemcitabine in patients with advanced pancreatic cancer. J Clin Oncol 2015;33:1475–81.
9. Marcu L, Olver I. Tirapazamine: from bench to clinical trials. Curr Clin Pharmacol 2006;1:71–9.
10. Evans JW, Chernikova SB, Kachnic LA, Banath JP, Sordet O, Delahoussaye YM, et al. Homologous recombination is the principal pathway for the repair of DNA damage induced by tirapazamine in mammalian cells. Cancer Res 2008;68:257–65.
11. Zeman EM, Brown JM, Lemmon MJ, Hirst VK, Lee WW. SR-4233: a new bioreductive agent with high selective toxicity for hypoxic mammalian cells. Int J Radiat Oncol Biol Phys 1986;12:1239–42.
12. Rischin D, Peters L, Fisher R, Macann A, Denham J, Poulsen M, et al. Tirapazamine, cisplatin, and radiation versus fluorouracil, cisplatin, and radiation in patients with locally advanced head and neck cancer: a randomized phase II trial of the Trans-Tasman Radiation Oncology Group (TROG 98.02). J Clin Oncol 2005;23:79–87.
13. von Pawel J, von Roemeling R, Gatzemeier U, Boyer M, Elisson LO, Clark P, et al. Tirapazamine plus cisplatin versus cisplatin in advanced non–small-cell lung cancer: a report of the international CATAPULT I study group. J Clin Oncol 2000;18:1351–9.
14. Rischin D, Peters LJ, O'Sullivan B, Giralt J, Fisher R, Yuen K, et al. Tirapazamine, cisplatin, and radiation versus cisplatin and radiation for advanced squamous cell carcinoma of the head and neck (TROG 02.02, HeadSTART): a phase III trial of the Trans-Tasman Radiation Oncology Group. J Clin Oncol 2010;28:2989–95.
15. Peters LJ, O'Sullivan B, Giralt J, Fitzgerald TJ, Trotti A, Bernier J, et al. Critical impact of radiotherapy protocol compliance and quality in the treatment of advanced head and neck cancer: results from TROG 02.02. J Clin Oncol 2010;28:2996–3001.
16. Rischin D, Young RJ, Fisher R, Fox SB, Le QT, Peters LJ, et al. Prognostic significance of p16INK4A and human papillomavirus in patients with oropharyngeal cancer treated on TROG 02.02 phase III trial. J Clin Oncol 2010;28:4142–8.
17. Rischin D, Hicks RJ, Fisher R, Binns D, Corry J, Porceddu S, et al. Prognostic significance of [^{18}F]-misonidazole positron emission tomography-detected tumor hypoxia in patients with advanced head and neck cancer randomly assigned to chemoradiation with or without tirapazamine: a substudy of Trans-Tasman Radiation Oncology Group Study 98.02. J Clin Oncol 2006;24:2098–104.
18. Trinkaus ME, Hicks RJ, Young RJ, Peters LJ, Solomon B, Bressel M, et al. Correlation of p16 status, hypoxic imaging using [^{18}F]-misonidazole positron emission tomography and outcome in patients with loco-regionally advanced head and neck cancer. J Med Imaging Radiat Oncol 2014;58:89–97.
19. Hicks KO, Fleming Y, Siim BG, Koch CJ, Wilson WR. Extravascular diffusion of tirapazamine: effect of metabolic consumption assessed using the multicellular layer model. Int J Radiat Oncol Biol Phys 1998;42:641–9.
20. Hicks KO, Pruijn FB, Sturman JR, Denny WA, Wilson WR. Multicellular resistance to tirapazamine is due to restricted extravascular transport: a pharmacokinetic/pharmacodynamic study in HT29 multicellular layer cultures. Cancer Res 2003;63:5970–7.
21. Hicks KO, Pruijn FB, Secomb TW, Hay MP, Hsu R, Brown JM, et al. Use of three-dimensional tissue cultures to model extravascular transport and predict *in vivo* activity of hypoxia-targeted anticancer drugs. J Natl Cancer Inst 2006;98:1118–28.
22. Hicks KO, Siim BG, Jaiswal JK, Pruijn FB, Fraser AM, Patel R, et al. Pharmacokinetic/pharmacodynamic modeling identifies SN30000 and SN29751 as tirapazamine analogues with improved tissue penetration and hypoxic cell killing in tumors. Clin Cancer Res 2010;16:4946–57.
23. Hunter FW, Wang J, Patel R, Hsu HL, Hickey AJR, Hay MP, et al. Homologous recombination repair-dependent cytotoxicity of the benzotriazine di-N-oxide CEN-209: comparison with other hypoxia-activated prodrugs. Biochem Pharmacol 2012;83:574–85.
24. Wang J, Foehrenbacher A, Su J, Patel R, Hay MP, Hicks KO, et al. The 2-nitroimidazole EF5 is a biomarker for oxidoreductases that activate the bioreductive prodrug CEN-209 under hypoxia. Clin Cancer Res 2012;18:1684–95.
25. Gu Y, Patterson AV, Atwell GJ, Chernikova SB, Brown JM, Thompson LH, et al. Roles of DNA repair and reductase activity in the cytotoxicity of the hypoxia-activated dinitrobenzamide mustard PR-104A. Mol Cancer Ther 2009;8:1714–23.
26. Hunter FW, Hsu HL, Su J, Pullen SM, Wilson WR, Wang J. Dual targeting of hypoxia and homologous recombination repair dysfunction in triple-negative breast cancer. Mol Cancer Ther 2014;13:2501–14.
27. Anderson RF, Yadav P, Patel D, Reynisson J, Tipparaju SR, Guise CP, et al. Characterisation of radicals formed by the triazine 1,4-dioxide hypoxia-activated prodrug, SN30000. Org Biomol Chem 2014;12:3386–92.
28. Duan JX, Jiao H, Kaizerman J, Stanton T, Evans JW, Lan L, et al. Potent and highly selective hypoxia-activated achiral phosphoramidate mustards as anticancer drugs. J Med Chem 2008;51:2412–20.
29. Yamamoto F, Oka H, Antoku S, Ichiya Y, Masuda K, Maeda M. Synthesis and characterization of lipophilic 1-[^{18}F]fluoroalkyl-2-nitroimidazoles for imaging hypoxia. Biol Pharm Bull 1999;22:590–7.
30. Su J, Gu Y, Pruijn FB, Smaill JB, Patterson AV, Guise CP, et al. Zinc finger nuclease knock-out of NADPH:cytochrome P450 oxidoreductase (POR) in human tumor cell lines demonstrates that hypoxia-activated prodrugs differ in POR dependence. J Biol Chem 2013;288:37138–53.
31. Guise CP, Abbattista MR, Tipparaju SR, Lambie NK, Su J, Li D, et al. Diflavin oxidoreductases activate the bioreductive prodrug PR-104A under hypoxia. Mol Pharmacol 2012;81:31–40.
32. Su J, Guise CP, Wilson WR. FSL-61 is a 6-nitroquinolone fluorogenic probe for one-electron reductases in hypoxic cells. Biochem J 2013;452:79–86.
33. Marcotte R, Brown KR, Suarez F, Sayad A, Karamboulas K, Krzyzanowski PM, et al. Essential gene profiles in breast, pancreatic, and ovarian cancer cells. Cancer Discov 2012;2:172–89.
34. Chia SK, Wykoff CC, Watson PH, Han C, Leek RD, Pastorek J, et al. Prognostic significance of a novel hypoxia-regulated marker, carbonic anhydrase IX, in invasive breast carcinoma. J Clin Oncol 2001;19:3660–8.
35. Echeverri CJ, Beachy PA, Baum B, Boutros M, Buchholz F, Chanda SK, et al. Minimizing the risk of reporting false positives in large-scale RNAi screens. Nat Methods 2006;3:777–9.
36. Hicks RJ, Rischin D, Fisher R, Binns D, Scott AM, Peters LJ. Utility of FMISO PET in advanced head and neck cancer treated with chemoradiation incorporating a hypoxia-targeting chemotherapy agent. Eur J Nucl Med Mol Imaging 2005;32:1384–91.
37. Cancer Genome Atlas Network. Comprehensive genomic characterization of head and neck squamous cell carcinomas. Nature 2015;517:576–82.
38. Dhani N, Milosevic M. Targeting tumoral hypoxia: finding opportunity in complexity. Future Oncol 2012;8:1065–8.
39. Peters L, Rischin D. Elusive goal of targeting tumor hypoxia for therapeutic gain. J Clin Oncol 2012;30:1741–3.
40. Guise CP, Wang AT, Theil A, Bridewell DJ, Wilson WR, Patterson AV. Identification of human reductases that activate the dinitrobenzamide mustard prodrug PR-104A: a role for NADPH:cytochrome P450 oxidoreductase under hypoxia. Biochem Pharmacol 2007;74:810–20.
41. Patterson AV, Saunders MP, Chinje EC, Talbot DC, Harris AL, Strafford IJ. Overexpression of human NADPH:cytochrome c (P450) reductase confers enhanced sensitivity to both tirapazamine (SR 4233) and RSU 1069. Br J Cancer 1997;76:1338–47.
42. Wang J, Guise CP, Dachs GU, Phung Y, Hsu AH, Lambie NK, et al. Identification of one-electron reductases that activate both the hypoxia prodrug SN30000 and diagnostic probe EF5. Biochem Pharmacol 2014;91:436–46.
43. Chandor A, Dijols S, Ramassamy B, Frapart Y, Mansuy D, Stuehr D, et al. Metabolic activation of the antitumor drug 5-(Aziridin-1-yl)-2,4-

Published OnlineFirst August 21, 2015; DOI: 10.1158/0008-5472.CAN-15-1107

dinitrobenzamide (CB1954) by NO synthases. Chem Res Toxicol 2008;21:836–43.
44. Hunter FW, Jaiswal JK, Hurley DG, Liyanage HD, McManaway SP, Gu Y, et al. The flavoprotein FOXRED2 reductively activates nitro-chloromethyl-benzindolines and other hypoxia-targeting prodrugs. Biochem Pharmacol 2014;89:224–35.
45. Cenas N, Prast S, Nivinskas H, Sarlauskas J, Arner ES. Interactions of nitroaromatic compounds with the mammalian selenoprotein thioredoxin reductase and the relation to induction of apoptosis in human cancer cells. J Biol Chem 2006;281:5593–603.
46. Seow HA, Penketh PG, Shyam K, Rockwell S, Sartorelli AC. 1,2-Bis(methylsulfonyl)-1-(2-chloroethyl)-2-[[1-(4-nitrophenyl)ethoxy]carbonyl]hydrazine: an anticancer agent targeting hypoxic cells. Proc Natl Acad Sci U S A 2005;102:9282–7.
47. Aboagye EO, Lewis AD, Tracy M, Workman P. Bioreductive metabolism of the novel fluorinated 2-nitroimidazole hypoxia probe N-(2-hydroxy-3,3,3-trifluoropropyl)-2-(2-nitroimidazolyl) acetamide (SR-4554). Biochem Pharmacol 1997;54:1217–24.
48. Eustace A, Mani N, Span PN, Irlam JJ, Taylor J, Betts GN, et al. A 26-gene hypoxia signature predicts benefit from hypoxia-modifying therapy in laryngeal cancer but not bladder cancer. Clin Cancer Res 2013;19:4879–88.
49. Toustrup K, Sørensen BS, Nordsmark M, Busk M, Wiuf C, Alsner J, et al. Development of a hypoxia gene expression classifier with predictive impact for hypoxic modification of radiotherapy in head and neck cancer. Cancer Res 2011;71:5923–31.
50. Shalem O, Sanjana NE, Hartenian E, Shi X, Scott DA, Mikkelsen TS, et al. Genome-scale CRISPR-Cas9 knockout screening in human cells. Science 2014;343:84–7.

Cancer Research
The Journal of Cancer Research (1916–1930) | The American Journal of Cancer (1931–1940)

AACR American Association for Cancer Research

Identification of P450 Oxidoreductase as a Major Determinant of Sensitivity to Hypoxia-Activated Prodrugs

Francis W. Hunter, Richard J. Young, Zvi Shalev, et al.

Cancer Res 2015;75:4211-4223. Published OnlineFirst August 21, 2015.